Electronic Supplementary Material (ESI) for Molecular Systems Design & Engineering.

Rationally designed foldameric adjuvants enhance antibiotic efficacy via promoting membrane hyperpolarization

Kaushik Nath Bhaumik[a],‡, Anasztázia Hetényi[a],‡, Gábor Olajos[a],‡, Ana Martins[b],‡, Réka Spohn[b], Lukács Németh[c], Balázs Jojart[c], Petra Szili[b,d] , Anett Dunai[b], Pramod K Jangir[b], Lejla Daruka[b,e], Imre Földesi[f], Diána Kata[e], Csaba Pál[b]*, Tamás A Martinek[a]*

[a.] *Department of Medical Chemistry, University of Szeged, Dóm tér 8, Szeged HU-6720, Hungary*
[b.] *Synthetic and Systems Biology Unit, Biological Research Centre, Eötvös Loránd Research Network (ELKH), Szeged, Hungary*
[c.] *Institute of Food Engineering, University of Szeged, Szeged, Hungary*
[d.] *Doctoral School of Multidisciplinary Medical Sciences, University of Szeged, Szeged, Hungary*
[e.] *Doctoral School of Biology, Faculty of Science and Informatics, University of Szeged, Szeged, Hungary*
[f.] *Department of Laboratory Medicine, University of Szeged, Szeged, Hungary*
‡These authors contributed equally to this work
E-mail: cpal@brc.hu, martinek.tamas@med.u-szeged.hu

Table of Contents

Methods

Table S1 Minimum inhibitory concentrations of PGLa, PGLb1 and PGLb2 against a panel of *E. coli* clinical isolates and their antibiotic resistant derivatives.

Table S2 Combination index (CI) values of peptide-antibiotic combinations on *E. coli* clinical isolates and the respective antibiotic-resistant strains.

Table S3. Calculation and result table for Job plot analysis

Table S4. Peptide contents of PGLa and analogues was measured with NanoDrop direct absorbance at 205 nm.

Fig. S1 Stepwise folding of the α-helix conformation observed for PGLa.

Fig. S2 Folding steps coupled to the desolvation of key residues according to molecular dynamics simulations.

Fig. S3 Chemical structure of the utilized β^3 amino acids

Fig. S4 Interaction of the sequences with membrane mimetics.

Fig. S5 Peptide-ampicillin interactions

Fig. S6 Impact of sub-inhibitory concentrations of PGLb1 and PGLb2 on antibiotic activity against moxifloxacin-resistant pathogenic strains.

Fig. S7 Impact of sub-inhibitory concentrations of PGLb1 and PGLb2 on antibiotic activity against *E. coli* BW 25113 mutants gyrA* (D87G) and gyrA* (S83L).

Fig. S8 Membrane polarization measurements for valinomycin (VAL) in presence of the K^+ (outside)/Na^+(inside) gradient.

Fig. S9 Membrane polarization measurements in LUVs without ion gradient.

Fig. S10 Ion gradient-dependent membrane polarization measurements with PGLb2 in LUVs.

Fig. S11 Time-dependent ^{35}Cl NMR measurements of the ion efflux with LUV in the presence of $Co(NO_3)_2$.

Fig. S12 Time-dependent ^{35}Cl NMR measurements for Prodigiosin.

Fig. S13 Time-dependent ^{35}Cl NMR measurements for Triton-X.

Fig. S14 AMPs do not aggregate the LUVs.

Fig. S15 ^1H-NMR (600 MHz, T = 310 K) titration spectra for PGLa with TBACl in DMSO-d_6.

Fig. S16 Plot of concentration of TBACl versus chemical shift of ^1H signal, fitted to 1:1 binding model of WinEQNMR2 program.

Fig. S17 ^1H-NMR titration curve of PGLa with TBACl in DMSO-d_6.

Fig. S18 Time-dependent ^{23}Na NMR measurements of the ion efflux on LUVs with valinomycin (VAL).

Characterization of compounds

Methods:

Folding mechanism of PGLa at the membrane-water interface. Altogether 36 simulations were performed. In 26 cases the simulation was stopped at 750 ns because we did not see any chance for folding of the peptide. For the 10 remaining cases, the simulation time was extended again for 375 ns, this brought us to an aggregate simulation time exceeding 30 μs.

Among the 36 simulations, we obtained complete folding of PGLa on the membrane surface only in one case (Figure S1). The folding of PGLa was followed by calculating the RMS value of αC atoms using a reference structure with ideal α-helix backbone dihedral values (Φ = -65º and Ψ = -39º) and depicted along with the alteration of N_p (number of peptide residues closer than 7.0 Å from the membrane) value.

There is a clear relationship between the N_p value and the conformational change of PGLa. During the first 350 ns, there is no stable contact with the membrane indicating by the fluctuation of N_p, in line with the large (> 4 Å) RMS fluctuation. Thereafter until 510-520 ns the RMS decreased linearly and stabilized at around 3 Å (with a fluctuation of ±1 Å) in the next 250 ns. After this temporarily stabilized state, a large drop was detected in the RMS value, and in the remaining part of the simulation, the RMS value became lower than 2.0 Å, indicating the folded state of PGLa.

According to the visual inspection of the time evolution of the secondary structure elements along the trajectory, we divided the peptide into three segments: GLY1-GLY7, ALA8-LYS15 and VAL16-LEU21.

The stepwise folding mechanism of PGLa was further analysed by calculating the number of water molecules in contact with the side chains (N_w) in the course of the simulations, except for glycine residues (G1, G7 and G11) where all atoms were considered (Figure S2). N_w was determined in the first solvation shell (O atoms closer than 3.5 Å to any peptide residue atoms).

Circular dichroism measurements. Measurements were performed using a Jasco J-1100 CD-spectrometer. Spectra were recorded by using a 1mm quartz cuvette, from 250 to 190 nm at a scan speed of 50 nm min^{-1}, with 6 accumulations. Compounds were dissolved in Na-phosphate buffer (10mM, pH 7.2) at 100 μg ml^{-1} concentrations. LUVs were prepared with the previously described method, but in Na-phosphate buffer (10mM, pH 7.2) and without NaCl. CD spectra were measured without and in the presence of 1 mM LUV. Solvent baseline was subtracted.

NMR measurements. First, the Na^+/K^+ exchange was measured with 100 mM NaCl in the intravesicular and 100 mM KCl in the extravesicular space of the LUVs (Figure 8). The anion transport was tested with the combination of 100 mM NaCl inside and 100 mM $NaNO_3$ outside. $Dy(PPP)_2^{7-}$ and $Co(NO_3)_2$ were used as ^{23}Na and ^{35}Cl chemical shift reagents outside, respectively[1,2] (Figure S8). The experimental setup was further validated by a selective anionophore prodigiosin (Figure S9)[3], and a membrane disrupting agent triton-x (Figure S10) (details given in SI).

Dynamic light scattering. Dynamic light scattering revealed that there was no AMPs-induced shift of the LUV size distribution curve. Anion (Cl^-) binding titrations were carried out by using NMR in solvents mimicking the membrane-water interface (DMSO). The curve fitting on the concentration-dependent NMR chemical shifts yielded dissociation constants of 5.82 mM, 6.08 mM, and 3.58 mM for PGLa, PGLb1, and PGLb2, respectively. The Job plot analyses showed a stoichiometry of 1:1 for all sequences (Table S3 and Figure S14). The mM interactions were against the low dissociation rate hypothesis, which would have occurred for tight binding (< 1 μM).

Anion binding analysis by ^{1}H-NMR titrations. ^{1}H-NMR titrations of the synthesized compounds (0.67 mM stock solution) in DMSO-d6 were performed by the subsequent addition of tetrabutylammonium chloride (0- 2 equiv.) as a Cl^- ion source or tetrabutylammonium phosphate monobase (0- 2 equiv.) as a $H_2PO_4^-$ ion source. The changes in chemical shift of the N-H protons of the NH-moieties were analysed. Significant extents of chemical shift (Δδ) of both N-H protons were observed. All ^{1}H NMR spectra were stacked by using the Topspin 3.5 software. The changes in chemical shift against the concentration of chloride ion were fitted by the WinEQNMR2 program using 1:1 binding model.[4] The dissociation constant (Kd) values were determined by taking the reciprocal of binding constant (Ka; as mentioned in WinEQNMR2 program). The following equation (Eq.-S1) was used to calculate the binding constant-

$$\delta_{cal} = \sum_{m=1}^{m=i} \sum_{n=0}^{n=j} \frac{\delta_{mn} \beta_{mn} m [M]^m [L]^n}{[M]_{total}} \quad \ldots\ldots\ldots\ldots\ldots\ldots \text{Eq.-S1}$$

Where, *M* represents the free, uncomplexed receptor and *L* is the ligand; δcalc, is the weighted average of the chemical shifts of the various *M*-containing species present, *MmLn*, and i and j represent the maximum values of m and n respectively.

Determination of anion binding stoichiometry by Job's plot [5]. The main stock solution of the host (compound) and the guest (TBACl) were prepared in DMSO-d6 solvent at 310 K. The concentration of the stock solution of both host and guest were fixed at 1 mM. The chemical shift values were recorded and the change of chemical shift of N-H proton of the NH moiety at δ = 8.334 ppm at different mole fraction of the Cl^- ion were listed in Table S3. The Job's plot was shown in Figure S14, which indicated a 1:1 binding Stoichiometry of the complex.

Table S1. Minimum inhibitory concentrations of PGLa, PGLb1 and PGLb2 against a panel of *E. coli* clinical isolates and their antibiotic resistant derivatives.

Minimum Inhibitory Concentration (mg.l^{-1})				
Strain	resistant to:	Peptide		
		PGLa	PGLb1	PGLb2
E. coli 0370	Wild type	2.5	100	25
	Ampicillin	2.5	50	25
	Nalidixic acid	2.5	25	12.5
E. coli 3538	Wild type	20.0	>200	>200
	Ampicillin	10.0	100	200
	Nalidixic acid	20.0	200	200
E. coli CFT073	Wild type	2.5	50	25
	Ampicillin	2.5	25	25
	Nalidixic acid	2.5	25	6.25

Table S2. Combination index (CI) values of peptide-antibiotic combinations on *E. coli* clinical isolates and the respective antibiotic-resistant strains. CI was estimated in *E. coli* 0370, *E. coli* 3538 and *E. coli* CFT073 strains and their corresponding nalidixic acid- and ampicillin-resistant derivatives. The cut-off values were CI≥1.14 for antagonism (orange); CI≤0.86 for synergism (blue); and 0.86<CI<1.14 for no interaction (grey). For details see Materials and Methods.

Combination Index (CI)					
Strain	resistant to:	Antibiotic	Peptide		
			PGLa	PGLb1	PGLb2
E. coli 0370	Wild type	Nalidixic acid	1.26	0.47	0.31
		Ampicillin	1.30	0.74	0.63
E. coli 0370	Nalidixic acid	Nalidixic acid	1.09	0.91	0.36
	Ampicillin	Ampicillin	0.96	0.66	0.45
E. coli 3538	Wild type	Nalidixic acid	0.75	0.45	0.44
		Ampicillin	0.94	0.96	0.85
E. coli 3538	Nalidixic acid	Nalidixic acid	1.01	0.55	0.46
	Ampicillin	Ampicillin	0.84	0.94	0.60
E. coli CFT073	Wild type	Nalidixic acid	1.08	0.48	0.44
		Ampicillin	1.10	0.85	0.74
E. coli CFT073	Nalidixic acid	Nalidixic acid	0.85	0.81	0.36
	Ampicillin	Ampicillin	0.91	0.61	0.62

Table S3. **Calculation and result table for Job plot analysis.**

Sample	Host conc ([H], mM)	Guest conc. ([G], mM)	[H]+[G] (mM)	[H]/([H]+[G])	δ of proton	Δδ	{[H]/([H]+[G])}*Δδ
1	0.1	0.9	1	0.1	8.3381	0.0041	0.00041
2	0.2	0.8	1	0.2	8.34	0.006	0.0012
3	0.3	0.7	1	0.3	8.34035	0.00635	0.001905
4	0.4	0.6	1	0.4	8.33935	0.00535	0.00214
5	0.5	0.5	1	0.5	8.3384	0.0044	0.0022
6	0.6	0.4	1	0.6	8.3375	0.0035	0.0021
7	0.7	0.3	1	0.7	8.33655	0.00255	0.001785
8	0.8	0.2	1	0.8	8.3357	0.0017	0.00136
9	0.9	0.1	1	0.9	8.33495	0.00095	0.000855
10	1	0	1	1	8.334	0	0

Table S4. Peptide contents of PGLa and analogues was measured with NanoDrop direct absorbance at 205 nm.

Sample	**Peptide Content (%)**
PGLa	57.77
PGLb1	42.30
PGLb2	59.40
PGLb3	59.22

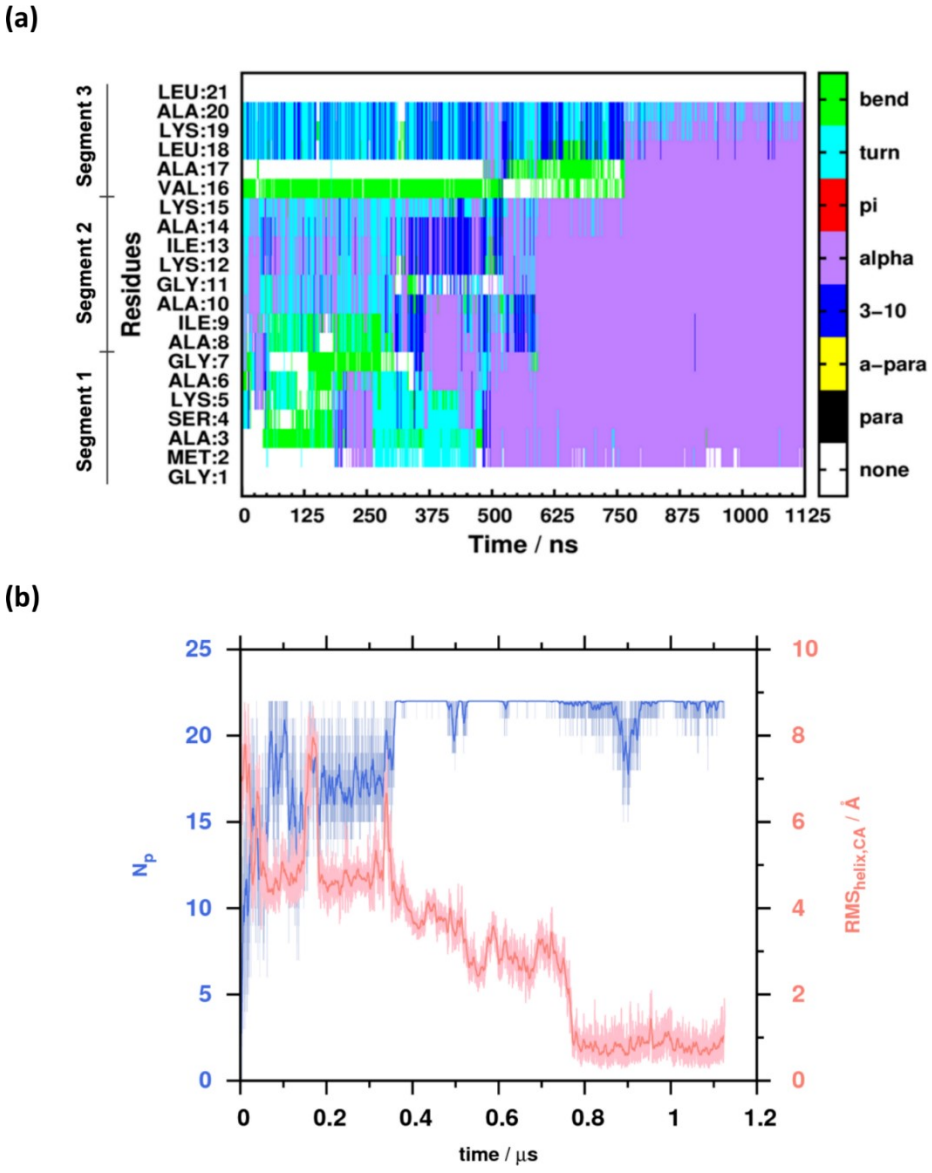

Fig. S1 (a) **Stepwise folding of the α-helix conformation observed for PGLa.** Helix nucleation starts from the N-terminal around 500 ns, after all Lys side chains had touched the membrane. (b) Time-dependence of membrane-residue contacts (N_p, blue) and the distance from the helical fold ($RMS_{helix,CA}$, red) values in the course of the simulation. Light color indicates actual, whereas dark color running averages over 1 ns.

(a)

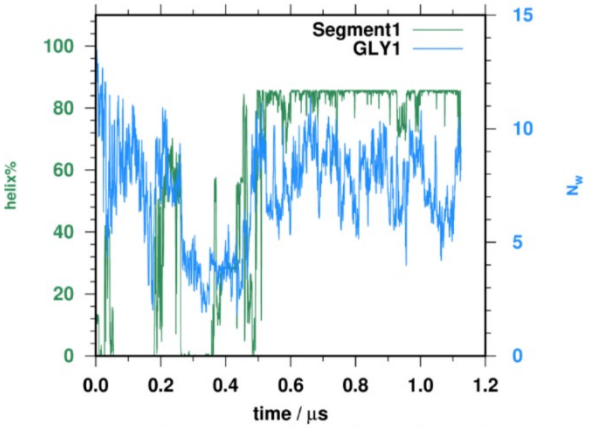
Segment1
GLY1
helix%
N_w
time / μs

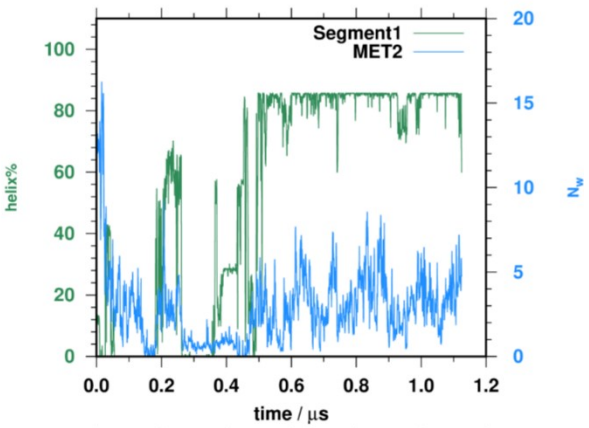
Segment1
MET2
helix%
N_w
time / μs

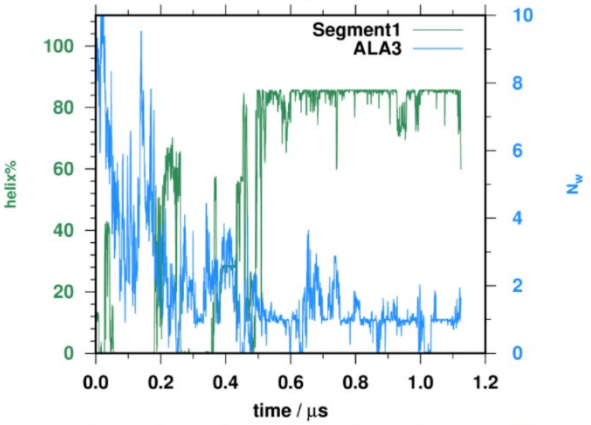
Segment1
ALA3
helix%
N_w
time / μs

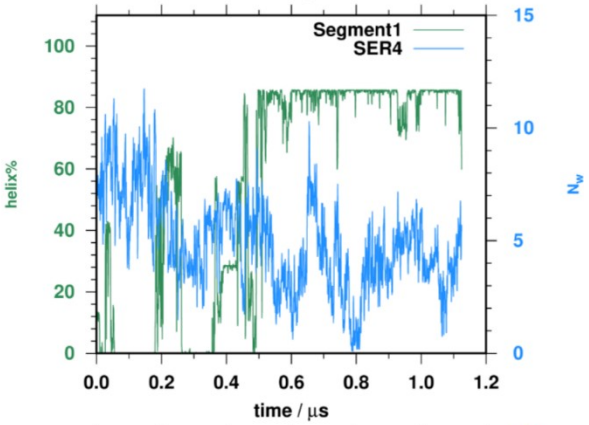
Segment1
SER4
helix%
N_w
time / μs

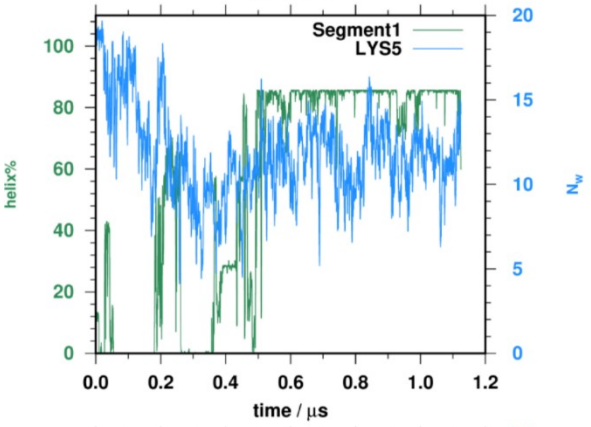
Segment1
LYS5
helix%
N_w
time / μs

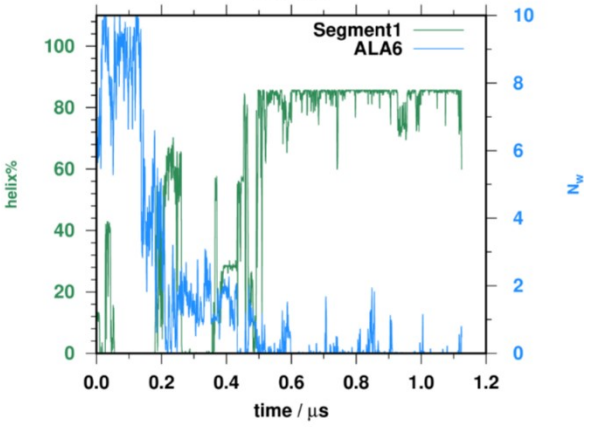
Segment1
ALA6
helix%
N_w
time / μs

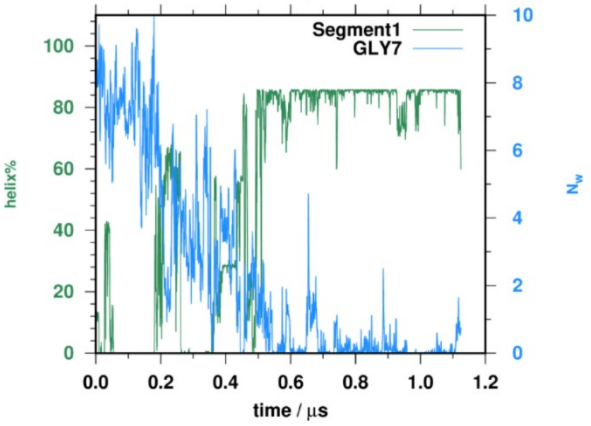
Segment1
GLY7
helix%
N_w
time / μs

(b)

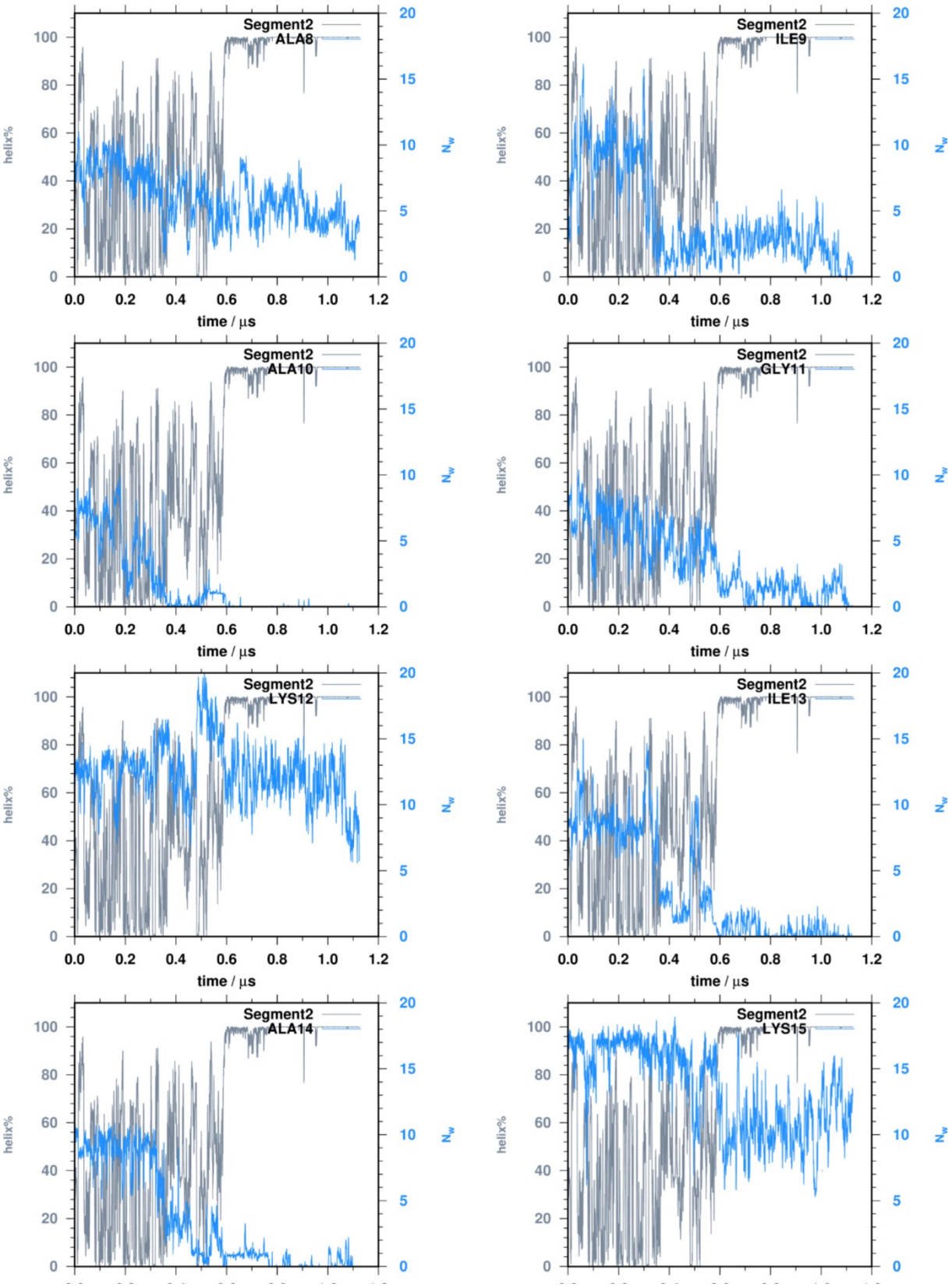
Segment2
ALA8
Segment2
ILE9
Segment2
ALA10
Segment2
GLY11
Segment2
LYS12
Segment2
ILE13
Segment2
ALA14
Segment2
LYS15
helix%
N_w
time / μs

(c)

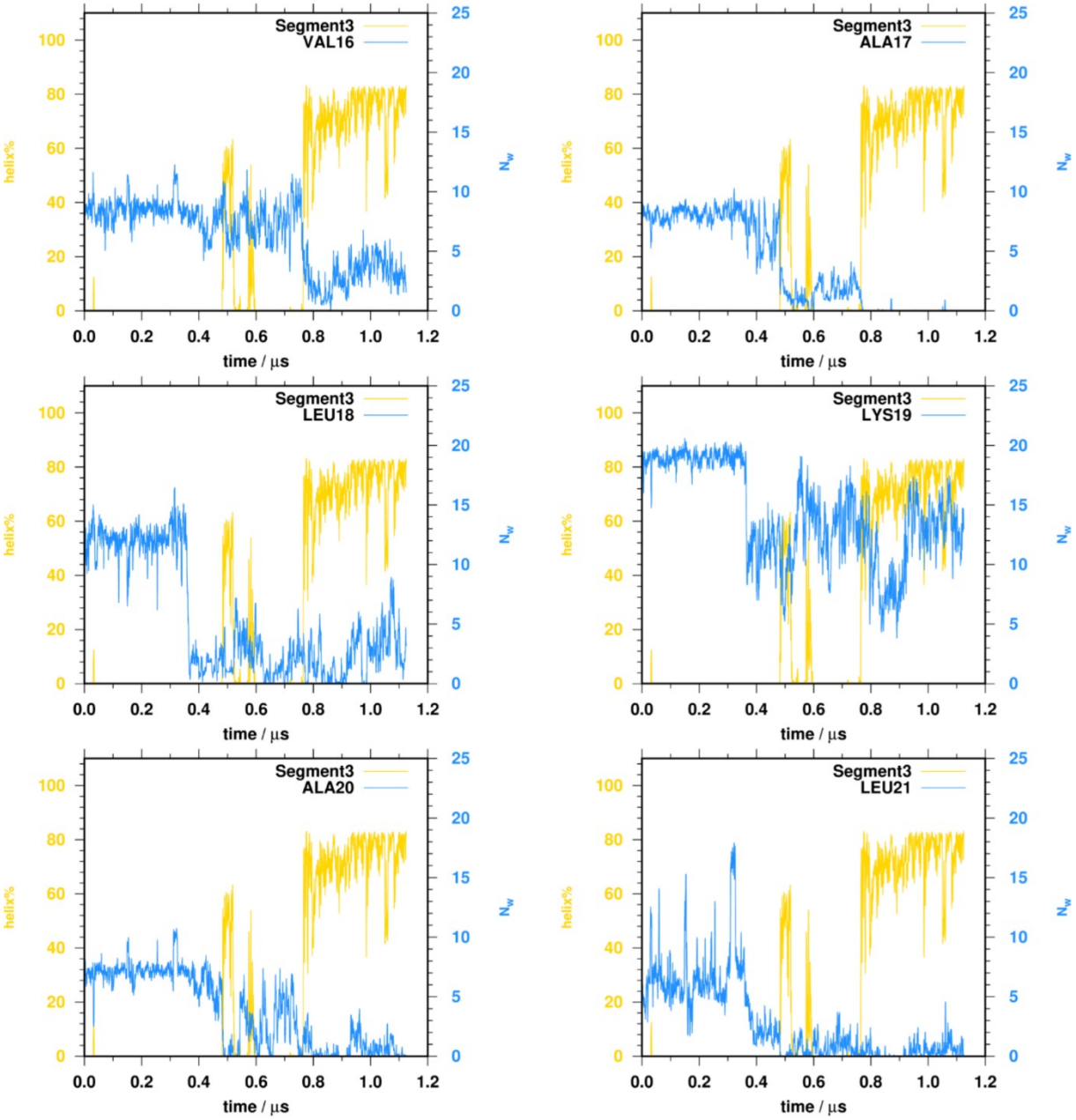

Fig. S2 Folding steps coupled to the desolvation of key residues according to molecular dynamics simulations. The change in α-helix propensity (green) and the number of water molecules (N_w) within 3.5 Å (blue) around the residues in segment 1 (**a**). The change in α-helix propensity (grey) and the number of water molecules within 3.5 Å (blue) around the residues in segment 2 (**b**). The change in α-helix propensity (yellow) and the number of water molecules within 3.5 Å (blue) around the residues in segment 3 (**c**).

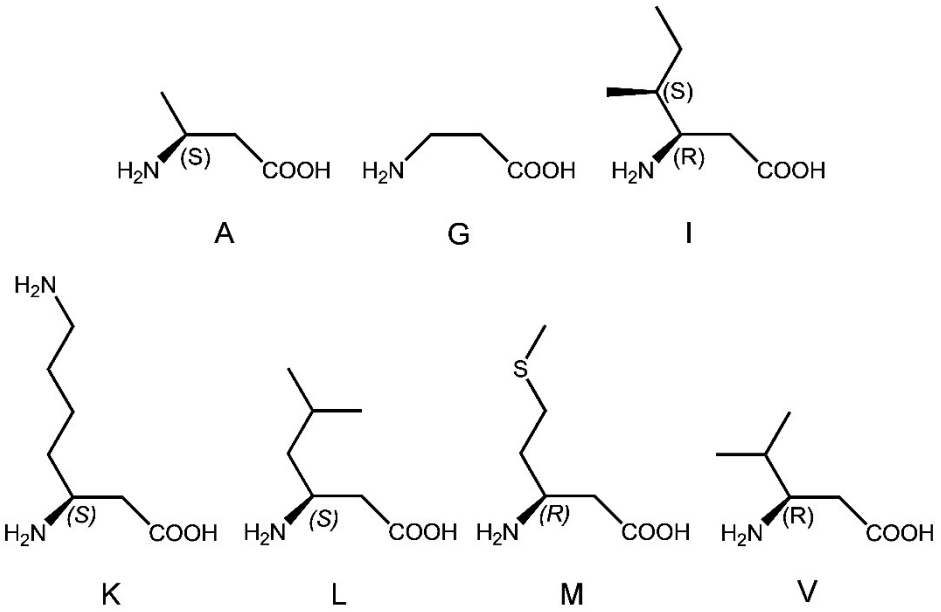

Fig. S3. Chemical structure of the utilized β–amino acids. All residues are β^3-homologues of the corresponding proteinogenic amino acids (except for glycine, where the corresponding homologue is beta-alanine).

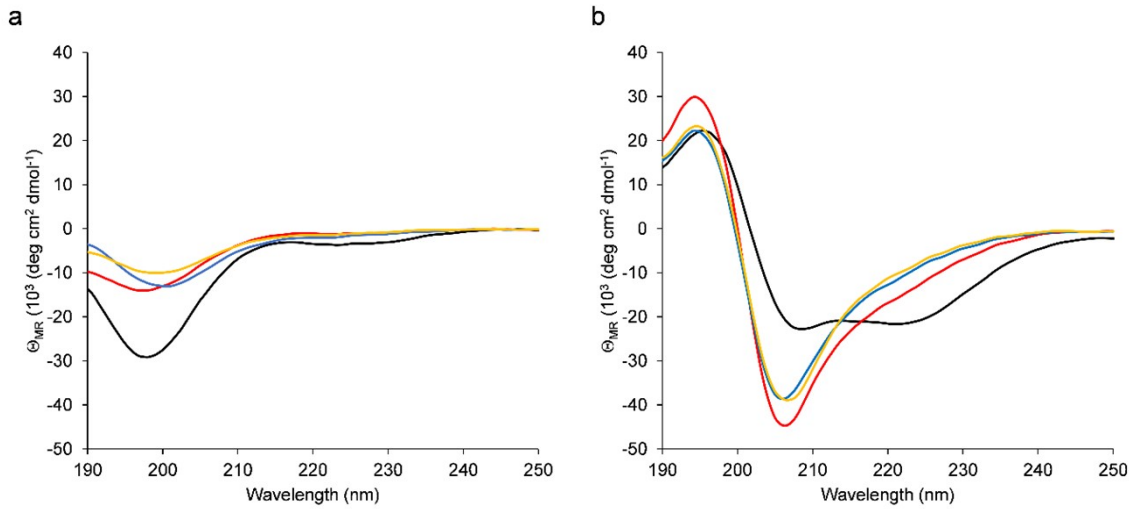

Fig. S4 Interaction of the sequences with membrane mimetics. CD spectra of PGLa (black), PGLb1 (blue), PGLb2 (red), and PGLb3 (yellow) without LUV (**a**) and in the presence of 1 mM DOPC/DOPG LUVs (**b**).

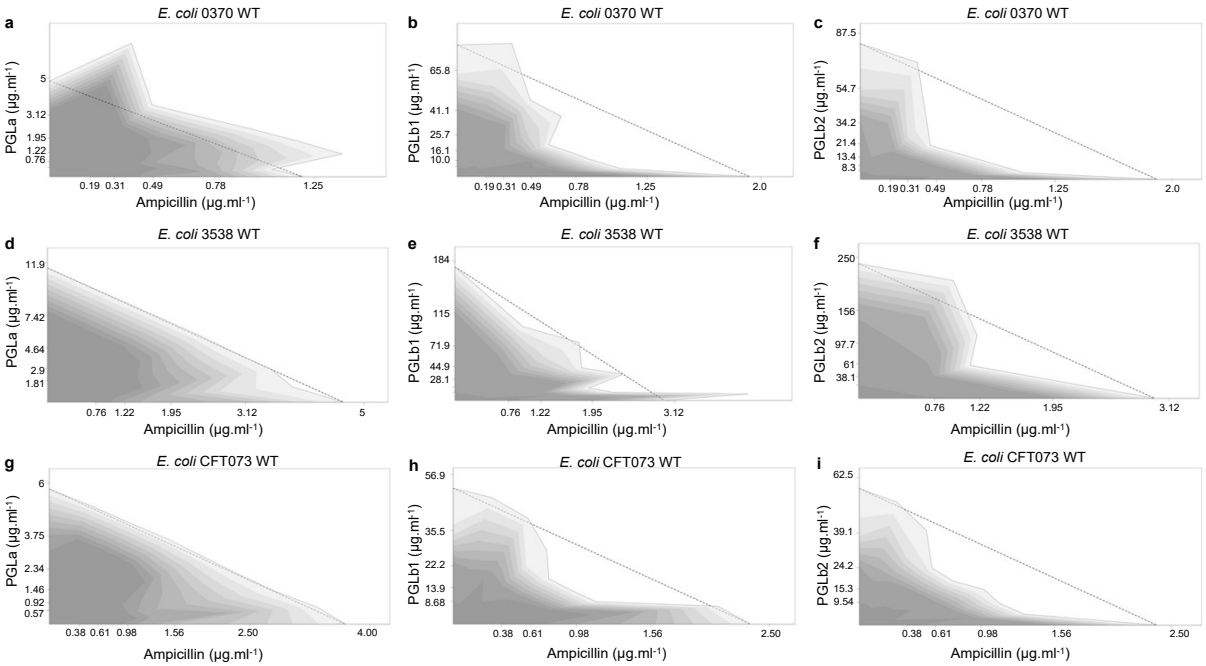

Fig. S4 Peptide-ampicillin interactions. Combination effect of PGLa, PGLb1 or PGLb2 with ampicillin against the wild-type *E. coli* 0370 (a-c)*, E. coli* 3538 (d-f), and *E. coli* CFT073 (g-i) strains. Dashed line represents no interaction calculated based on the Loewe additivity model (see Materials and Methods). Growth rate is represented in the combination space by the shade of the grey color, with darker shades denoting higher growth rates.

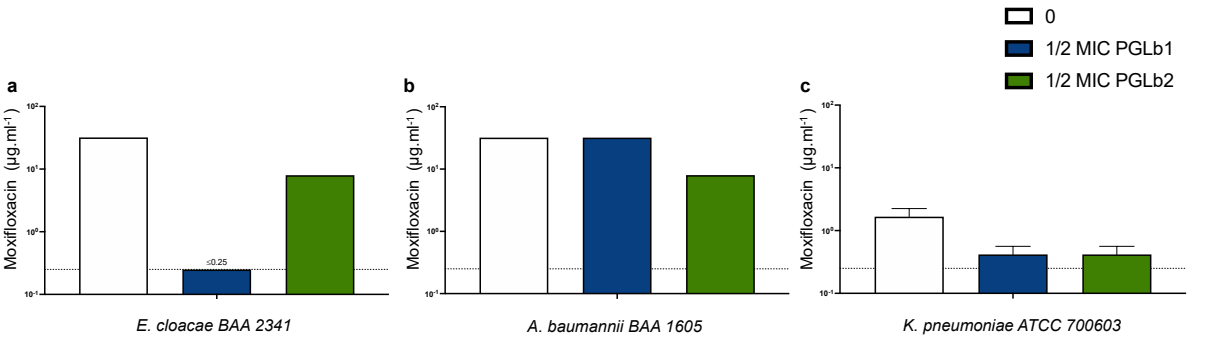

Fig. S6. Impact of sub-inhibitory concentrations of PGLb1 and PGLb2 on antibiotic activity against moxifloxacin-resistant pathogenic strains. The MIC of moxifloxacin (MOX) was measured in *Enterobacter cloacae* BAA2341 (**a**), *Acinetobacter baumannii* BAA 1605 (**b**), and *Klebsiella pneumonia ATCC 700603* (**c**) in the presence of ½ of the peptide MIC against each strain. None of the peptide concentrations, when applied alone, affected the growth of the strains. Dashed line represents the EUCAST suggested break point for MOX,[6] i.e. if MOX MIC is under or equal to 0.25 mg.l^{-1} the strain is considered susceptible to this antibiotic. Data in this figure is representative of at least 2 biological replicates. Note: MIC of PGLb1 and PGLb2 against these strains is >256mg.l^{-1} and therefore the concentrations 256mg.l^{-1} was considered as ½ MIC.

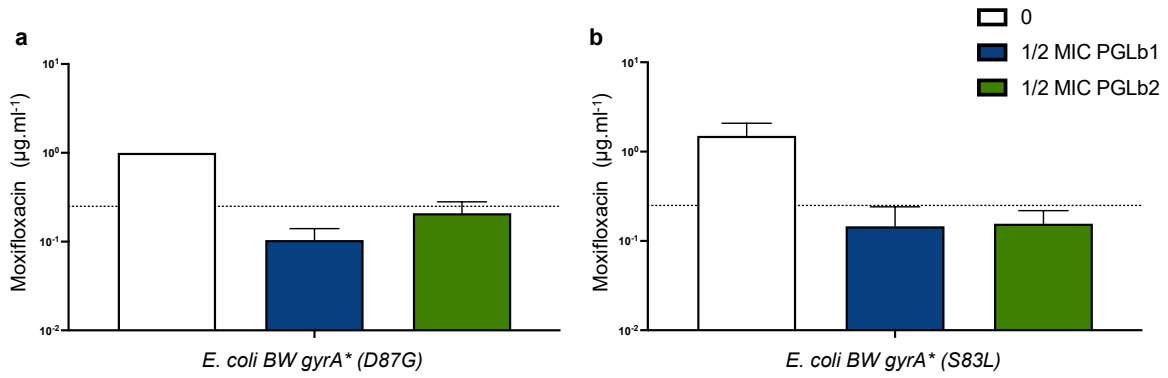

Fig. S7. Impact of sub-inhibitory concentrations of PGLb1 and PGLb2 on antibiotic activity against *E. coli* BW 25113 mutants gyrA* (D87G) and gyrA* (S83L). The MIC of moxifloxacin (MOX) was measured in gyrA* (D87G) (**a**) and gyrA* (S83L) (**b**) mutants in the presence of ½ of the peptide MIC against each strain. None of the peptide concentrations, when applied alone, affected the growth of the strains expect for the PGLa on the D87G mutant. Dashed line represents the EUCAST suggested break point for MOX,[6].e. if MOX MIC is under or equal to 0.25 mg.l^{-1} the strain is considered susceptible to this antibiotic. Data in this figure is representative of at least 2 biological replicates. Note: MIC of PGLb1 and PGLb2 against these strains is >256mg.l^{-1} and therefore the concentrations 256mg.l^{-1} was considered as ½ MIC.

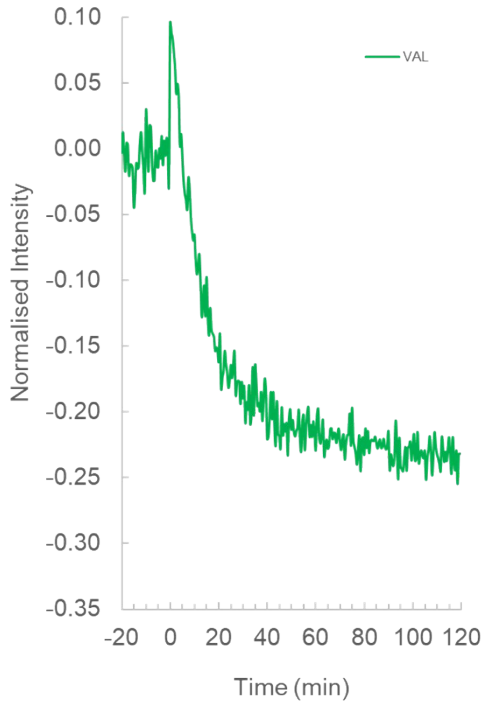

Fig. S8 Membrane polarization measurements for valinomycin (VAL) in presence of the K$^+$(outside)/Na$^+$(inside) gradient. The relative fluorescence level changes of the membrane potential-dependent dye oxonol VI was monitored with 100 mM NaCl in the intra- and 100 mM KCl in the extravesicular space.

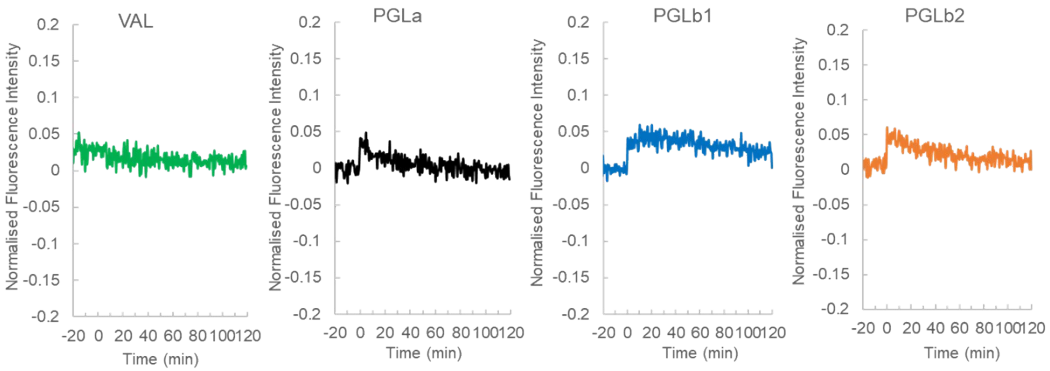

Fig. S9 Membrane polarization measurements in LUVs without ion gradient. The relative fluorescence level changes of the membrane potential dependent dye oxonol VI was monitored. Peptide-induced membrane potential with 100 mM NaCl in the intra- and in the extravesicular space. Curves for valinomycin (VAL), PGLa, PGLb1, and PGLb2 are represented with green, black, blue, red and orange, respectively.

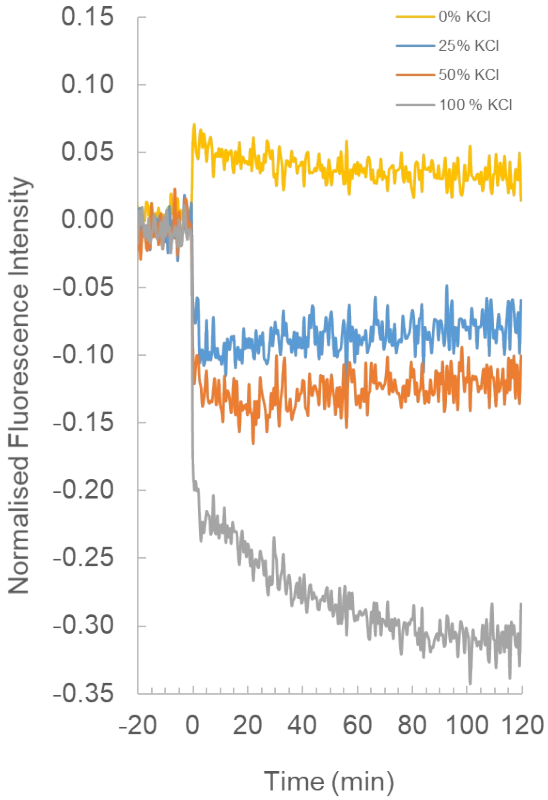

Fig. S10 Ion gradient-dependent membrane polarization measurements with PGLb2 in LUVs. The relative fluorescence level changes of the membrane potential dependent dye oxonol VI was monitored. PGLb2-induced membrane potential change in the Na^+/K^+ exchange. There was constant 100 mM NaCl in the intravesicular space. In the extravesicular space, the following compositions were applied: and 100 mM NaCl – 0 mM KCl (yellow), 75 mM NaCl – 25 mM KCl (blue), 50 mM NaCl – 50 mM KCl (orange), 0 mM NaCl – 100 mM KCl (grey).

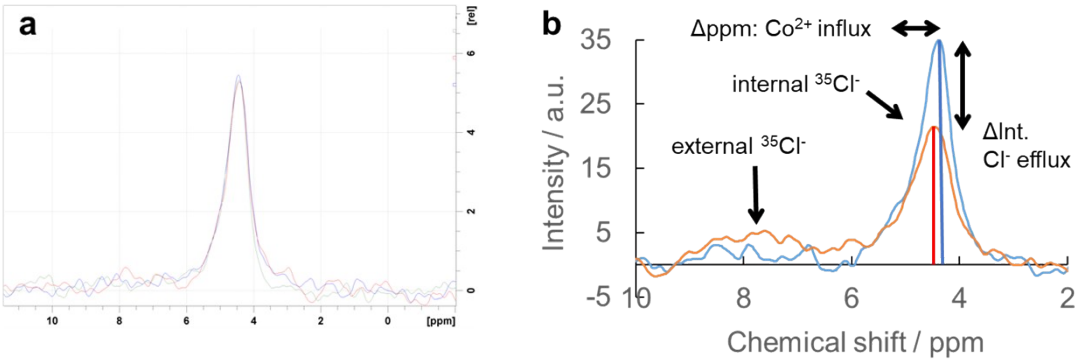

Fig. S11 Time-dependent ^{35}Cl NMR measurements of the ion efflux with LUV in the presence of $Co(NO_3)_2$. There is no intensity change without peptide (a) Theory of the ^{35}Cl measurements in the present of shift reagent. The extent of the Co^{2+} transport can be estimated from the difference between the pure chemical shift without Co^{2+} and the average chemical shift of the broadening and shifting signal (b).

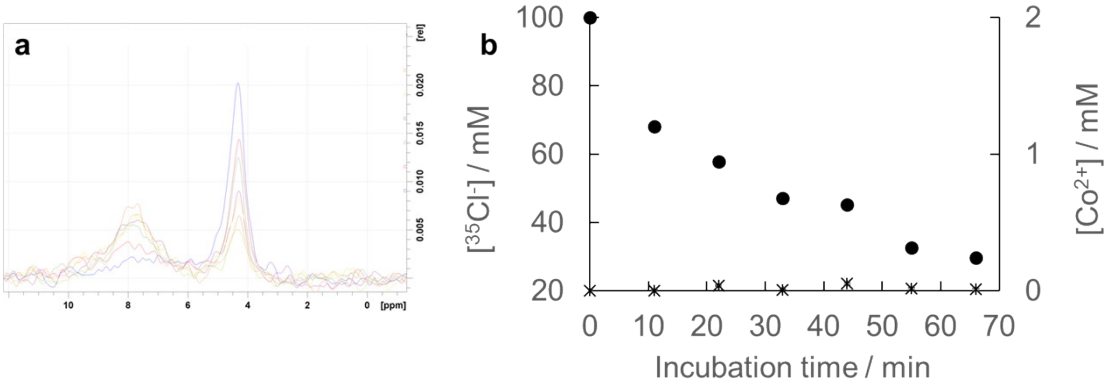

Fig. S12 Time-dependent ^{35}Cl NMR measurements for Prodigiosin. Upon adding the pure anionophore prodigiosin, a decrease of the internal signal at 4.5 ppm was recorded without any resonance shift and line broadening, which was in accord with the pore-free anion specific transport keeping the Co^{2+} outside of the LUVs. The external broad signal at around 8 ppm increased simultaneously.

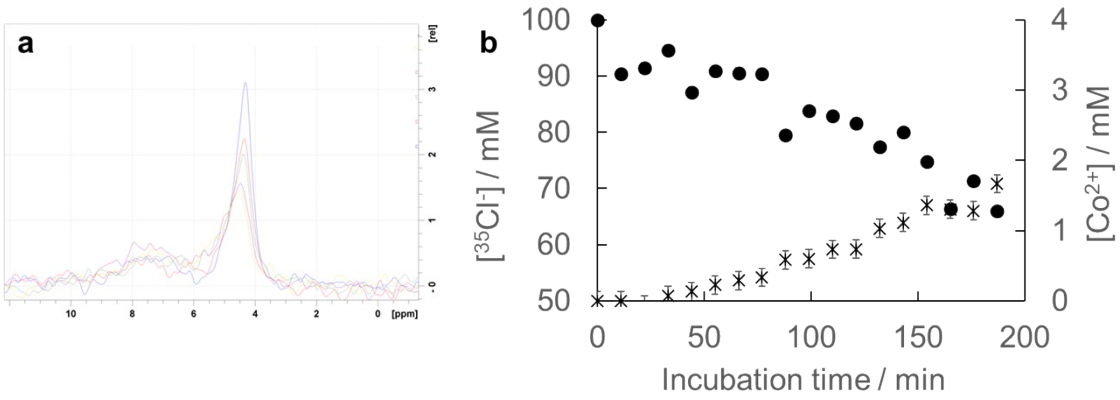

Fig. S13 Time-dependent ^{35}Cl NMR measurements for Triton-X. Triton-X as a pore forming agent caused overall downfield shift and broadening because of the Co^{2+} influx through the pores. Intensity decrease for the inside Cl^- resonance was observed in parallel.

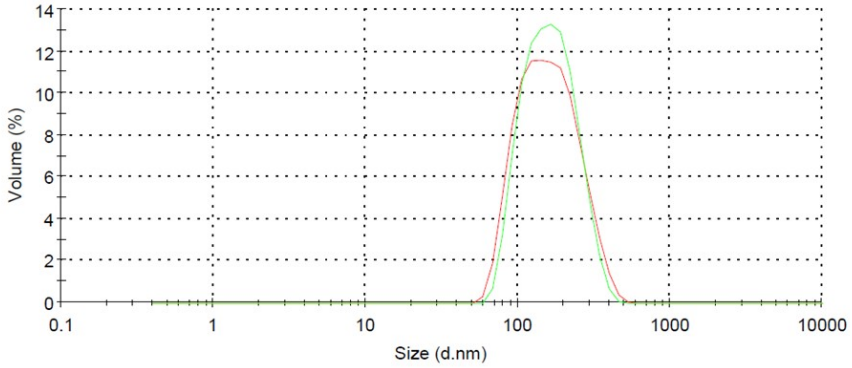

Fig. S14 AMPs do not aggregate the LUVs. Distribution of LUV size determined by dynamic light scattering before (green) and 2 hours after addition of 5 ?g/ml PGLa (red).

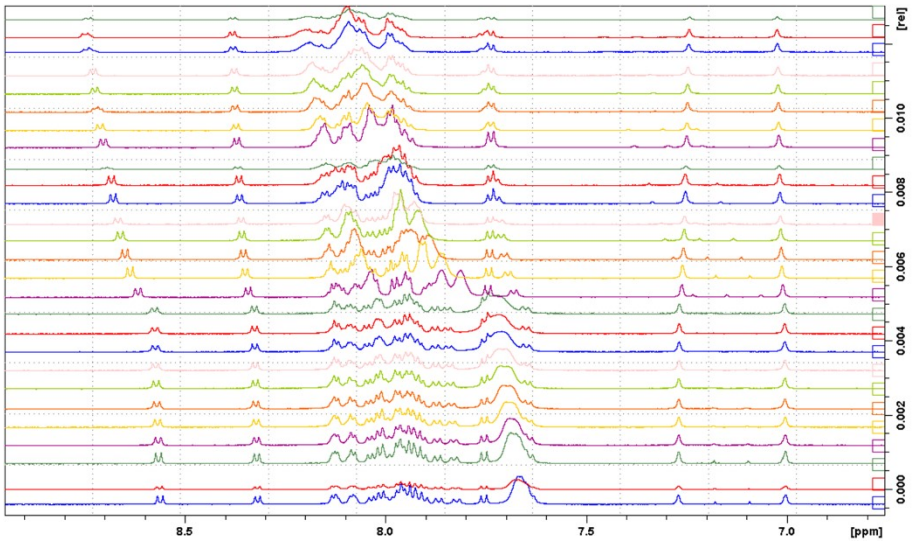

Fig. S15 ^{1}H-NMR (600 MHz, T = 310 K) titration spectra for PGLa with TBACl in DMSO-d_6.

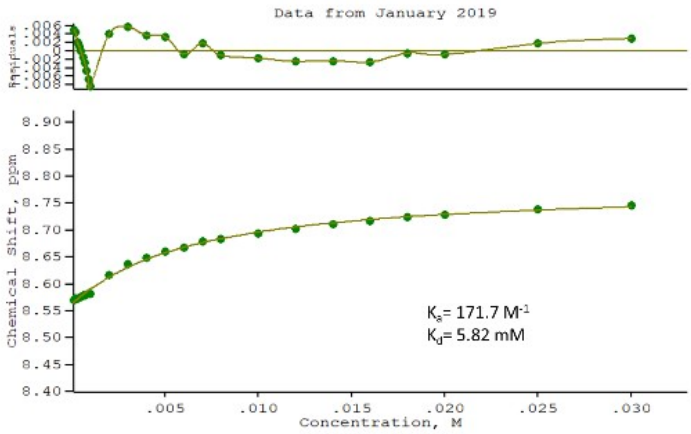

Fig. S16 Plot of concentration of TBACl versus chemical shift of ^{1}H signal, fitted to 1:1 binding model of WinEQNMR2 program.

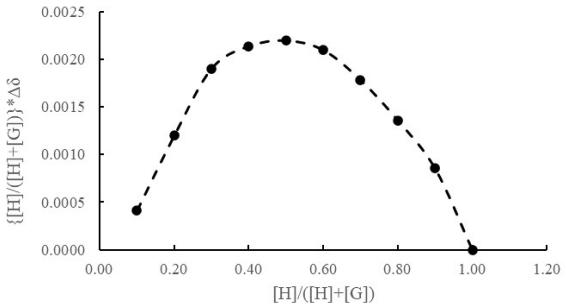

Fig. S17 ^{1}H-NMR titration curve of PGLa with TBACl in DMSO-d_6 solvent by varying mole fraction of PGLa (according to Table S3).

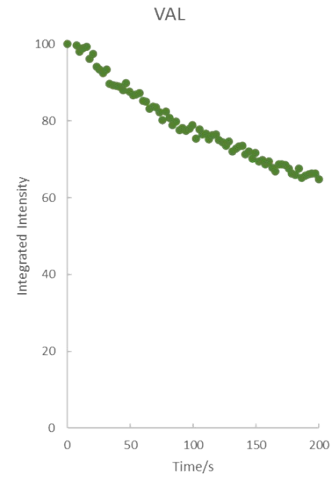

Fig. S18 Time-dependent ^{23}Na NMR measurements of the ion efflux on LUVs with **valinomycin** (VAL).

Characterization of compounds

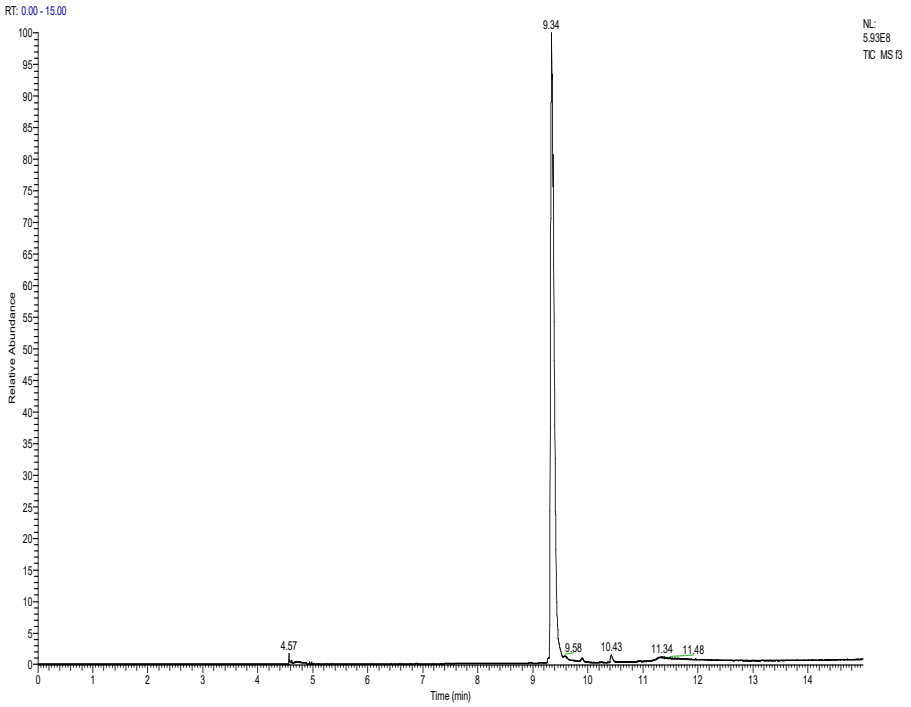

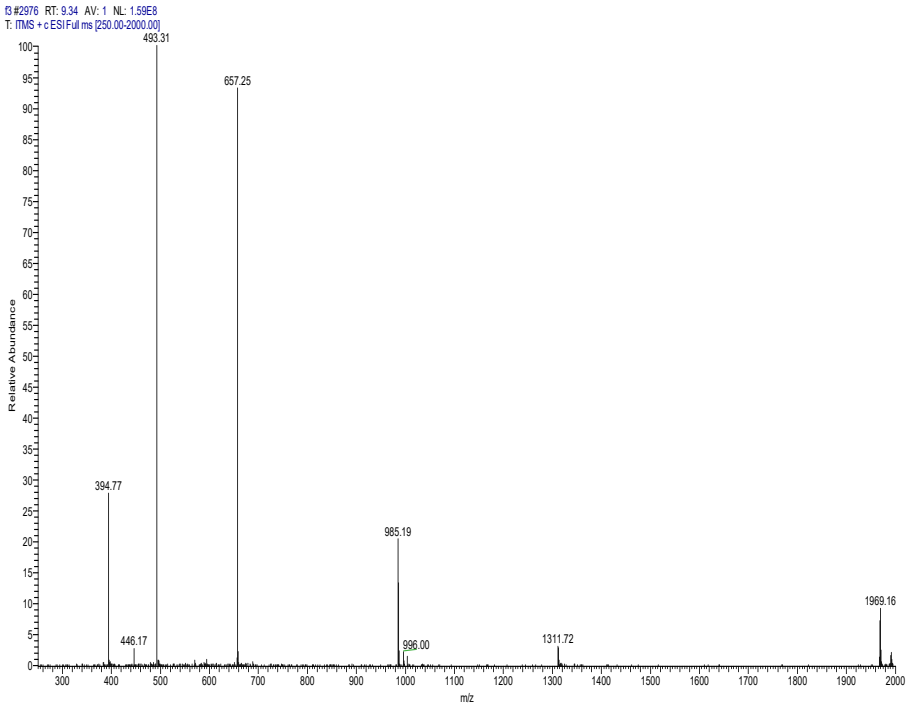

PGLa. MW: 1968.4. Expected m/z values: **[M+H]** $^{+}$:1969.4; **[M+2H]**$^{2+}$: 985.2; **[M+3H]**$^{3+}$: 657.1 **[M+4H]**$^{4+}$: 493.1

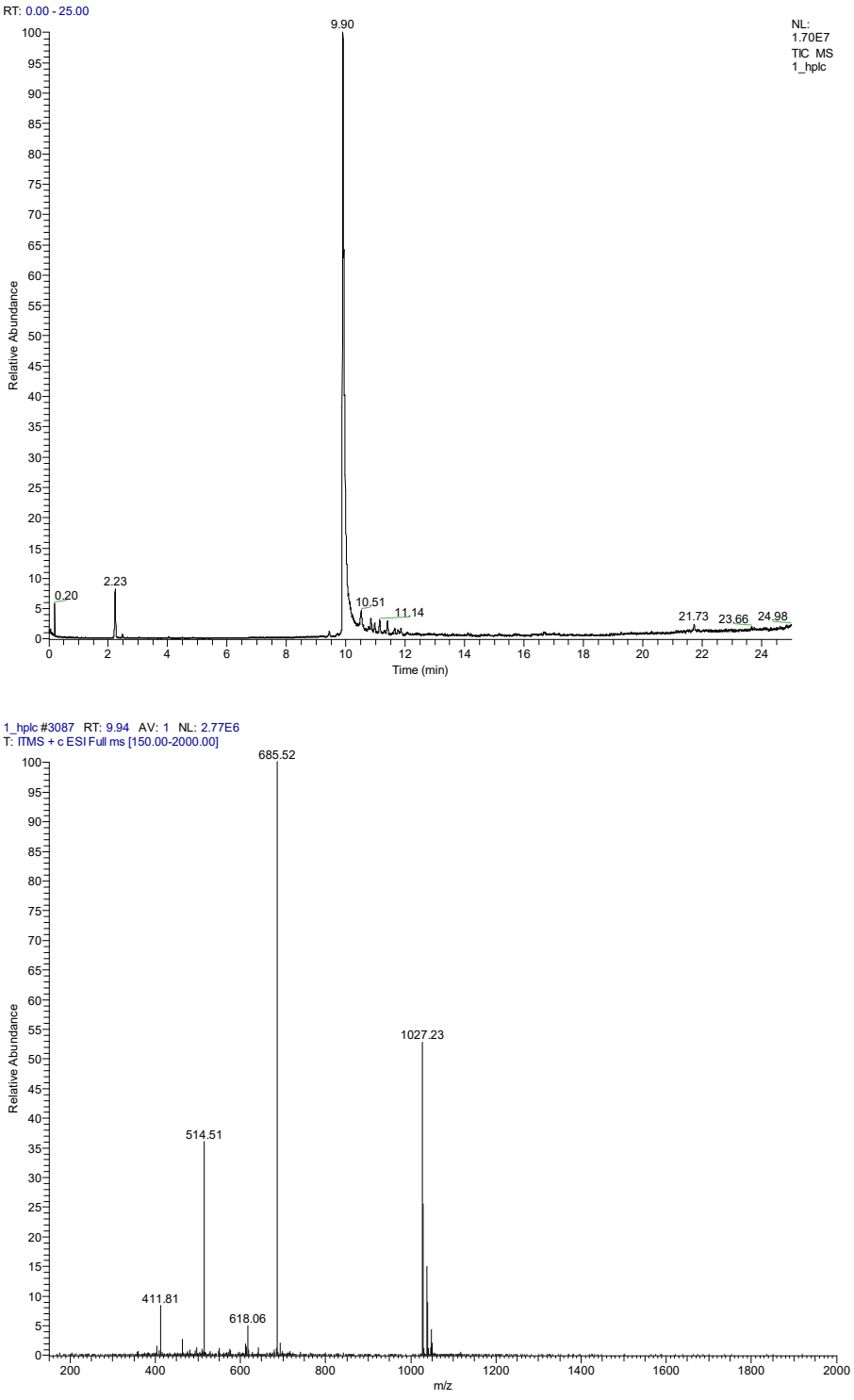

PGLb1. MW: 2052.6, Expected m/z values: **[M+2H]$^{2+}$**: 1027.3; **[M+3H]$^{3+}$**: 685.2; **[M+4H]$^{4+}$**: 514.2

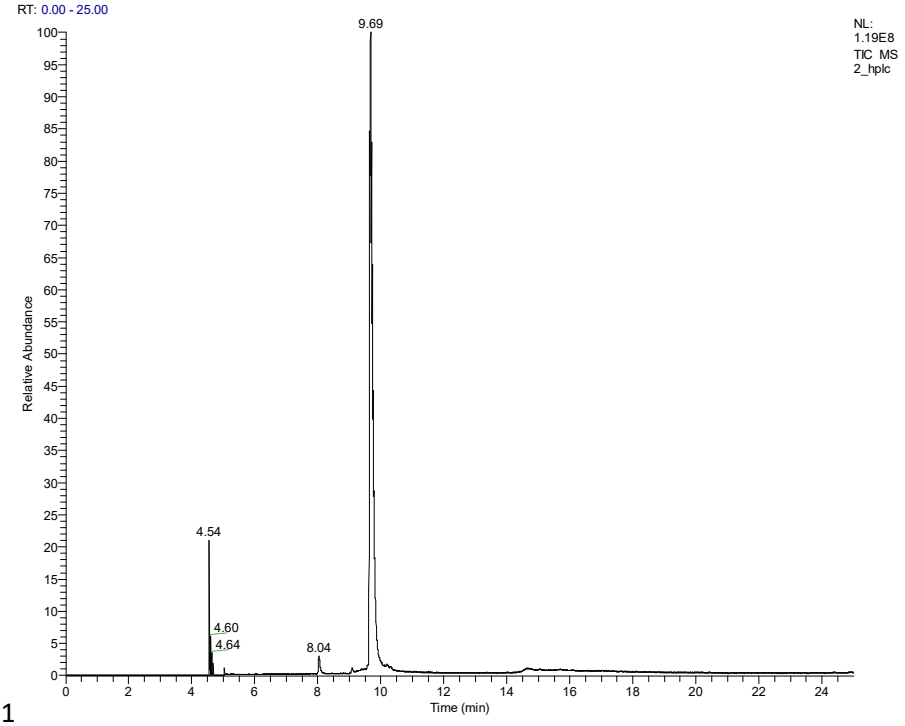

1

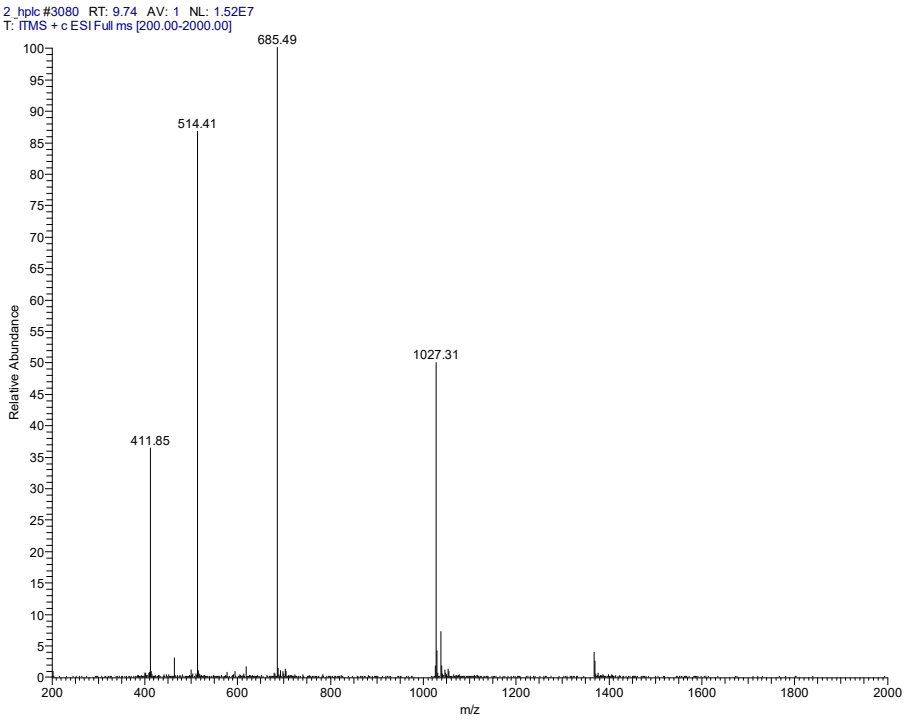

PGLb2. MW: 2052.6, Expected m/z values: **[M+2H]$^{2+}$**: 1027.3; **[M+3H]$^{3+}$**: 685.2; **[M+4H]$^{4+}$**: 514.2

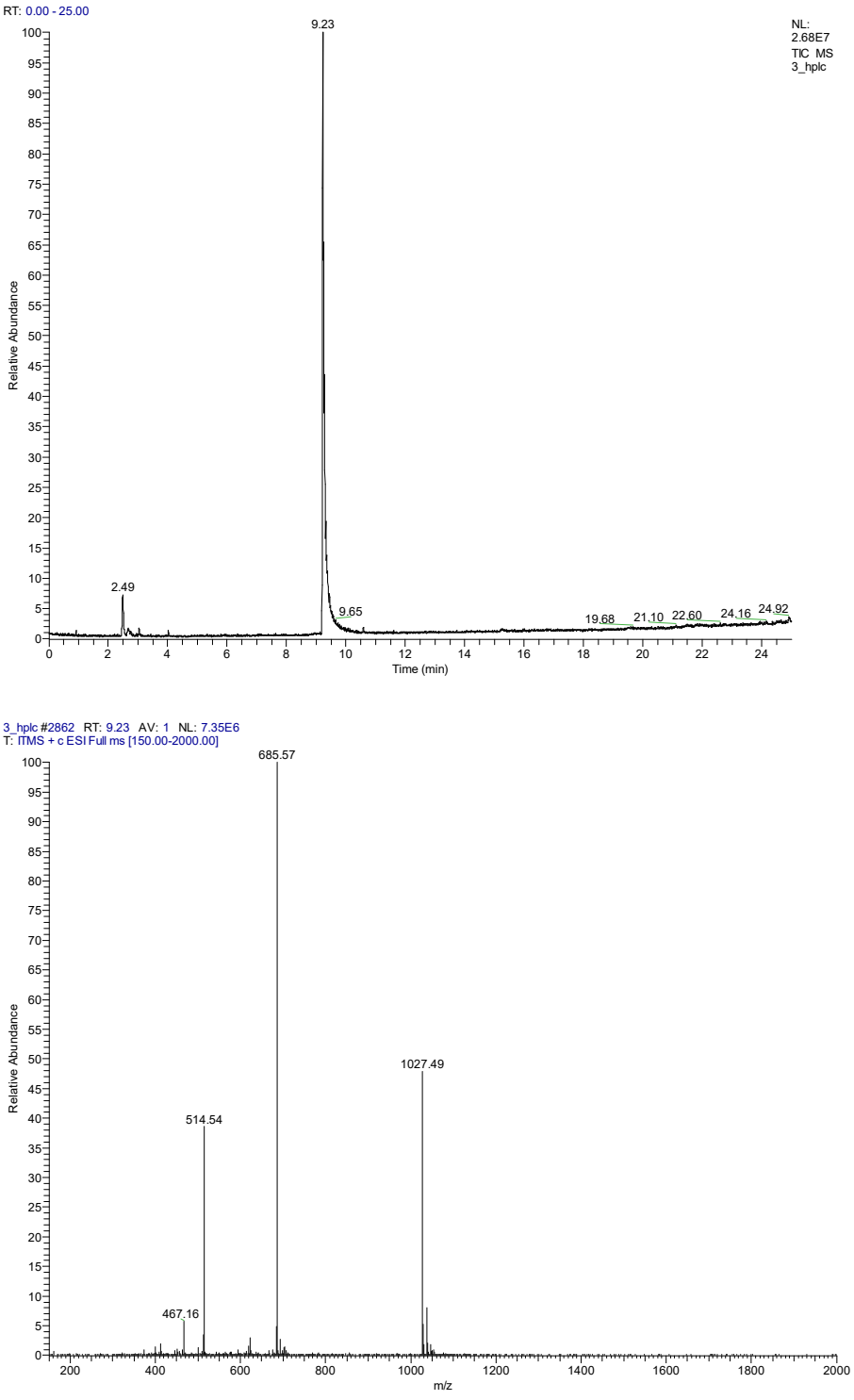

PGLb3. MW: 2052.6, Expected m/z values: **[M+2H]$^{2+}$**: 1027.3; **[M+3H]$^{3+}$**: 685.2; **[M+4H]$^{4+}$**: 514.2

Reference

1. A. R. Waldeck and P. W. Kuchel, *Biophysical Journal*, 1993, **64**, 1445-1455.
2. Y. Shacharhill and R. G. Shulman, *Biochemistry*, 1992, **31**, 6272-6278.
3. N. Akhtar, A. Saha, V. Kumar, N. Pradhan, S. Panda, S. Morla, S. Kumar and D. Manna, *Acs Applied Materials & Interfaces*, 2018, **10**, 33803-33813.
4. T. J. Jentsch, C. A. Hubner and J. C. Fuhrmann, *Nature Cell Biology*, 2004, **6**, 1039-1047.
5. T. Saha, M. S. Hossain, D. Saha, M. Lahiri and P. Talukdar, *Journal of the American Chemical Society*, 2016, **138**, 7558-7567.
6. E. Committee, *Journal*, 2021.